Biointerface Research in Applied Chemistry
Open-Access Journal (ISSN: 2069-5837)

Article
Volume 16, Issue 2, 2026, 50
https://doi.org/10.33263/BRIAC162.050

Molecular Simulation of SnC Nanosensor for Transport of Soft Metal Cations (Li^+, Na^+, K^+) across Biological Interfaces

Fatemeh Mollaamin [1,*], Majid Monajjemi [2]

[1] Department of Biomedical Engineering, Faculty of Engineering and Architecture, Kastamonu University, Kastamonu, Turkey
[2] Department of Biology, Faculty of Science, Kastamonu University, Kastamonu, Turkey
* Correspondence: fmollaamin@kastamonu.edu.tr;

Received: 14.09.2025; Accepted: 27.10.2025; Published: 15.04.2026

Abstract: Tin carbide (SnC) based nanostructures are distinctive materials with unique compositional, structural, optical, and electronic properties with exceptional band structure, moderate surface area, and exceptional thermal and chemical stability. Because of these properties, SnC-based nanomaterials have shown promising applications and higher performance in the biological arena. Functionalizing of Li^+, Na^+, K^+ cations can augment the negative atomic charge of C2, C3, C7–C12, C14, C15, C17, C18, C22–C27, C29, C30 as electron acceptors in $SnLi^+C$, $SnNa^+C$ and SnK^+C nanoclusters. $SnLi^+C$, $SnNa^+C$, SnK^+C nanoclusters have shown the steepest maximums TDOS surrounding –0.30, –0.40, –0.50, and –0.60 a.u. owing to the covalent bond between Li^+, Na^+, K^+ cations and SnC nanostructure with a maximum density of state of ≈ 12. The layered tin carbide improved by alkali metal ions of lithium (1+), sodium (1+), and potassium (1+) has indicated the structural stability of Li^+-, Na^+-, and K^+-ion heteroclusters through the reported stability energies. Finally, the unresolved issues, plausible challenges, current status, and future perspectives for the development and design of SnC have been summarized and are expected to promote a clinical path for the medical sector and human well-being.

Keywords: tin carbide nanocage; monovalent ions transport; cell membrane; molecular simulation.

1. Introduction

Today, it has been theoretically proven that two-dimensional graphene-like carbides, such as silicon carbide and germanium carbide monolayers, decorated with alkaline and transition-metal atoms, are promising candidates for hydrogen storage [1–6]. In this work, a theoretical study of the adsorption of hydrogen molecules on 2DSnC decorated with alkali metal (AM) atoms, such as Li, Na, and K, is reported, and the suitability of these decorated monolayers for hydrogen storage is discussed [7–9].

The majority of tin complexes are effective against a wide range of different disorders, including convulsions, tumors, cancer, malaria, tuberculosis, and diabetes. The majority of the tin complex exhibits drug-like antibacterial and antifungal properties. Tin complexes have greater activity than free ligands like macrocyclic and Schiff bases [10].

The tin compound $SnCl_2C_{34}H_{32}N_4$ gives a sharp signal at δ-576 ppm in the ^{119}Sn NMR spectrum, below the reported value for tri-coordinated hydrated tin (II) chloride. But in the case of four coordination number of tin complexes show square pyramidal geometry [11,12].

The triphenyltin (IV) complexes with 2-thiobarbituric acid have IC_{50} values of 0.06–0.2 μM toward various tumor cell lines, and the tricyclohexyltin (IV) complexes contain IC_{50} values of 0.15–1.41 Mn for a number of human tumor cell lines. Therefore, the inorganic tin (IV) complexes 1–3 are potential chemotherapeutic candidates to avoid the pollution problem of the organotin drugs [13].

In addition, the scientists applied first-principles simulations to determine the stability, electrical, and photocatalytic properties of a SnC/SnS_2 heterojunction. Analysis of its work function showed that the SnC/SnS_2 heterojunction has a built-in electric field pointing from the SnC monolayer to the SnS2 monolayer. The band edge position and the differential charge density indicate that the SnC/SnS_2 heterostructure exhibits a Z-scheme photocatalytic mechanism. It is found that the band gap and light absorption of the heterojunction can be effectively tuned by biaxial strain. These results demonstrate that the fabricated SnC/SnS_2 heterojunction has significant photocatalysis potential [14,15].

We have studied the structural and electronic attributes of $SnLi^+C$, $SnNa^+C$, and SnK^+C nanoclusters using state-of-the-art computational techniques (Figure 1a,b,c).

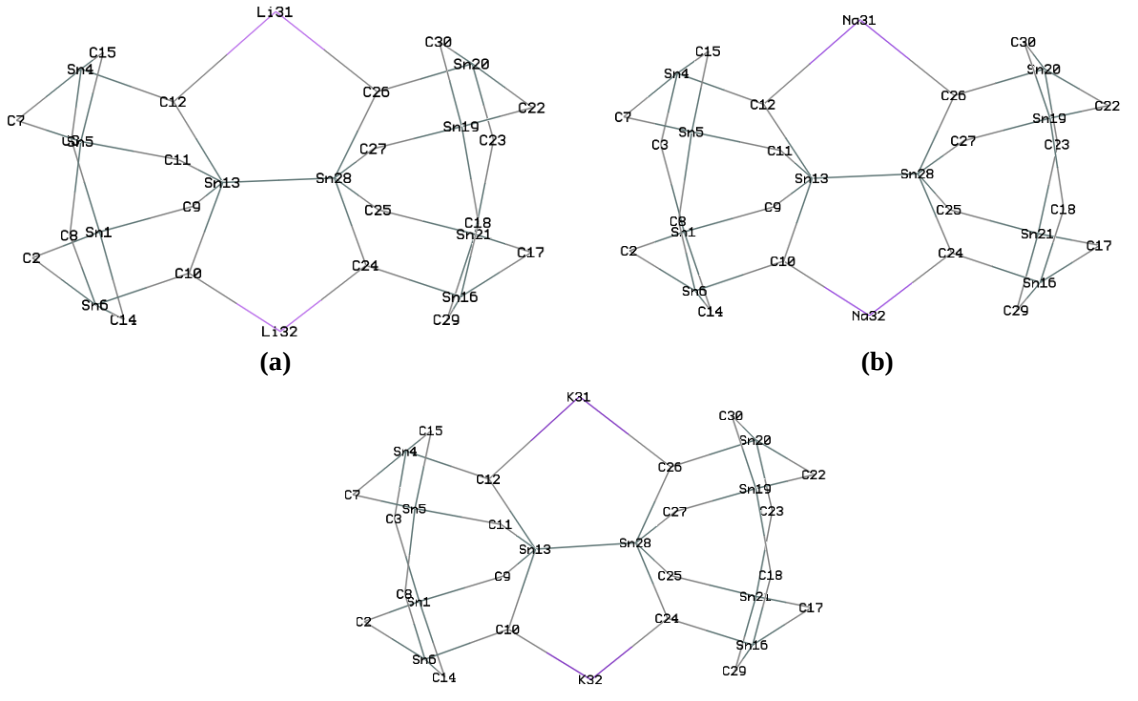

Figure 1. Optimized nanoclusters of **(a)** $SnLi^+C$; **(b)** $SnNa^+C$; **(c)** SnK^+C.

2. Materials and Methods

The aim of this study is to transport alkali metal ions of Li^+, Na^+, and K^+ by SnC nanocages towards the formation of $SnLi^+C$, $SnNa^+C$, and SnK^+C complexes (Scheme 1), which can increase the ion transfer in the cell membrane [16–19].

The analysis of Bader charge parameter [20] has been illustrated for Ion transport by hybrid clusters of $SnLi^+C$, $SnNa^+C$, and SnK^+C complexes with multiplicity of +1 by Gaussian 16 revision C.01 [21] and GaussView 6.1 programs [22].

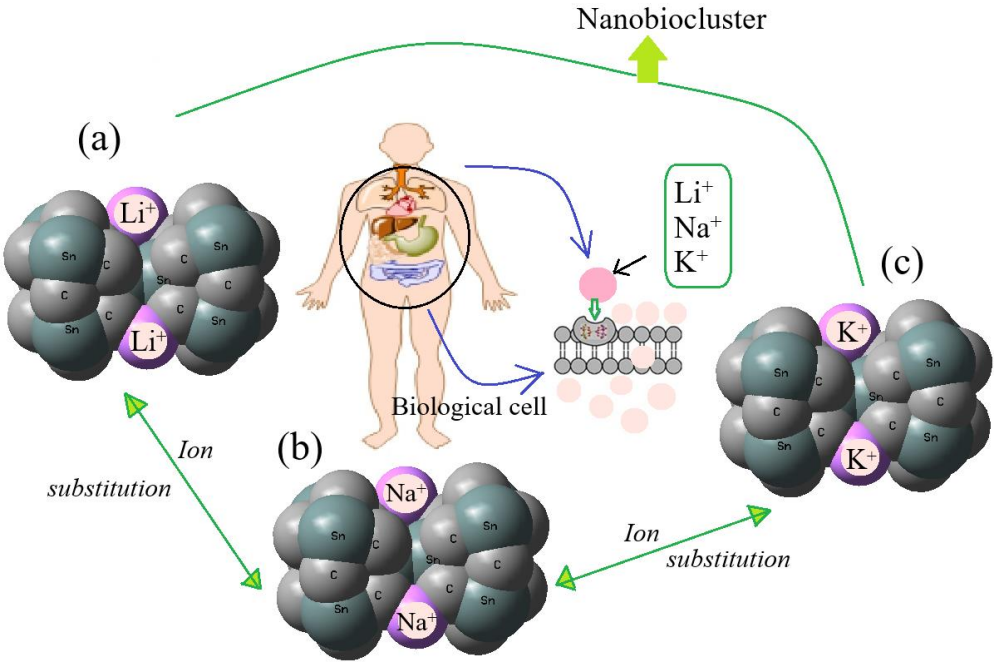

Scheme 1. Adding Li^+, Na^+, and K^+ to SnC nanocluster and formation of **(a)** $SnLi^+C$; **(b)** $SnNa^+C$; **(c)** SnK^+C complexes towards ion transport in biological cells.

The $Li^+/Na^+/K^+$ insertion might also result in the cleavage of some C–Li^+, C–Na^+, or C–K^+ bonds in the SnC nanocluster (Figure 1a, b, c). At the same time, the Li^+, Na^+, or K^+ cations could react rapidly with tin or carbon of SnC nanocluster to form $SnLi^+C$, $SnNa^+C$, and SnK^+C heteroclusters.

3. Results and Discussion

3.1. Charge density differences analysis.

In Figure 2(a,b,c), charge density differences (CDD) [23] have been shown for $SnLi^+C$, $SnNa^+C$, and SnK^+C nanoclusters. Moreover, the elements of C2, C3, C7–C12, C14, C15, C17, C18, C22–C27, C29, C30 from $SnLi^+C$, $SnNa^+C$, and SnK^+C nanoclusters have displayed the vibration about –12 to +9 Bohr (Figure 2a,b,c).

The charge distribution has been illustrated during alkali metal ions captured by SnC nanostructure towards the formation of $SnLi^+C$, $SnNa^+C$, and SnK^+C nanoclusters, respectively (Table 1).

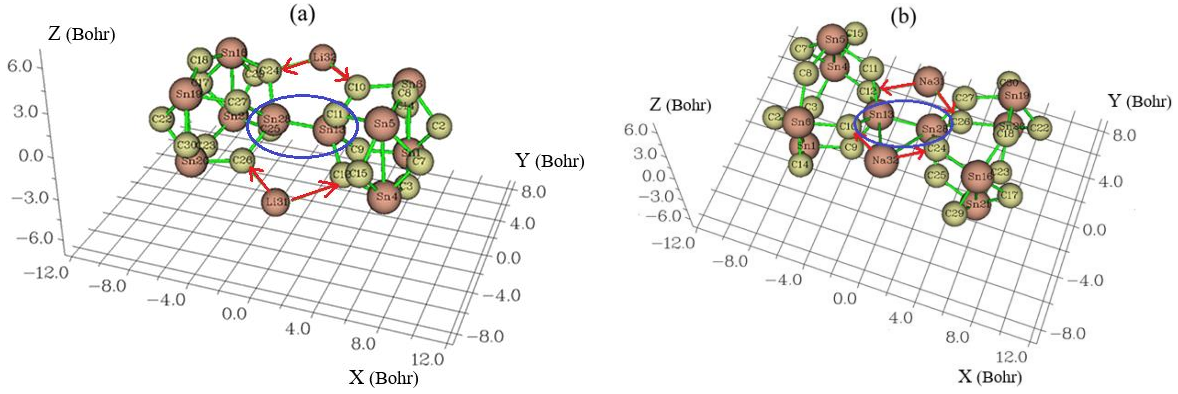

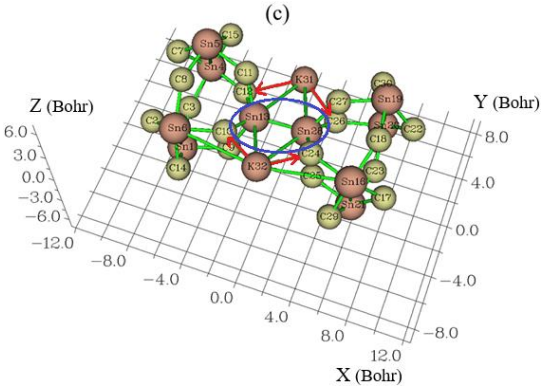

Figure 2. CDD graphs for **(a)** $SnLi^+C$; **(b)** $SnNa^+C$; **(c)** SnK^+C nanoclusters.

Table 1. The atomic charge (Q/coulomb) for $SnLi^+C$, $SnNa^+C$ and SnK^+C nanoclusters.

$SnLi^+C$		$SnNa^+C$		SnK^+C	
Atom/Ion	**Q**	**Atom/Ion**	**Q**	**Atom/Ion**	**Q**
Sn1	0.4767	Sn1	0.4829	Sn1	0.4511
C2	–0.3183	C2	–0.3227	C2	-0.3434
C3	–0.1790	C3	–0.1825	C3	-0.1630
Sn4	0.4706	Sn4	0.4704	Sn4	0.4485
Sn5	0.4638	Sn5	0.4714	Sn5	0.4850
Sn6	0.5113	Sn6	0.5534	Sn6	0.5678
C7	–0.3102	C7	–0.3107	C7	-0.3273
C8	–0.1559	C8	–0.1500	C8	-0.1794
C9	–0.3352	C9	–0.3276	C9	-0.3091
C10	–0.7357	C10	–0.6994	C10	-0.9351
C11	–0.3444	C11	–0.3427	C11	-0.2682
C12	–0.7635	C12	–0.7655	C12	-0.8307
Sn13	1.4424	Sn13	1.4300	Sn13	1.1959
C14	–0.3032	C14	–0.3191	C14	-0.2949
C15	–0.3108	C15	–0.3304	C15	-0.3156
Sn16	0.5585	Sn16	0.5969	Sn16	0.5715
C17	–0.3216	C17	–0.3219	C17	-0.3155
C18	–0.1694	C18	–0.1683	C18	-0.1911
Sn19	0.4356	Sn19	0.4417	Sn19	0.4305
Sn20	0.4845	Sn20	0.4840	Sn20	0.4677
Sn21	0.4658	Sn21	0.4769	Sn21	0.4552
C22	–0.3189	C22	–0.3188	C22	-0.3025
C23	–0.1495	C23	–0.1521	C23	-0.1659
C24	–0.7049	C24	–0.6645	C24	-0.8797
C25	–0.3237	C25	–0.3286	C25	-0.2838
C26	–0.7209	C26	–0.7239	C26	-0.7893
C27	–0.4179	C27	–0.4077	C27	-0.3248
Sn28	1.3792	Sn28	1.3973	Sn28	1.1998
C29	–0.3228	C29	–0.3493	C29	-0.3582
C30	–0.3155	C30	–0.3329	C30	-0.334
Li^+31	0.5219	Na^+31	0.5196	K^+31	0.7966
Li^+32	0.3115	Na^+32	0.1943	K^+32	0.8429

Functionalizing of Li^+, Na^+, K^+ cations can augment the negative atomic charge of C2, C3, C7–C12, C14, C15, C17, C18, C22–C27, C29, C30 as electron acceptors in $SnLi^+C$, $SnNa^+C$ and SnK^+C nanoclusters (Figure 3a,b,c).

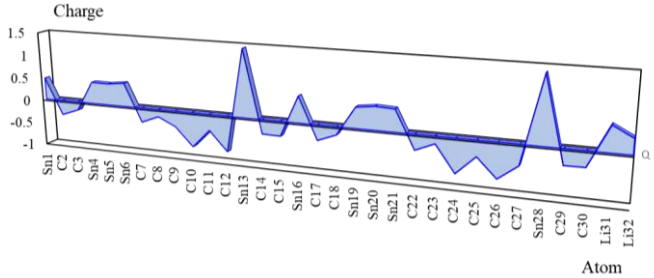

(a)

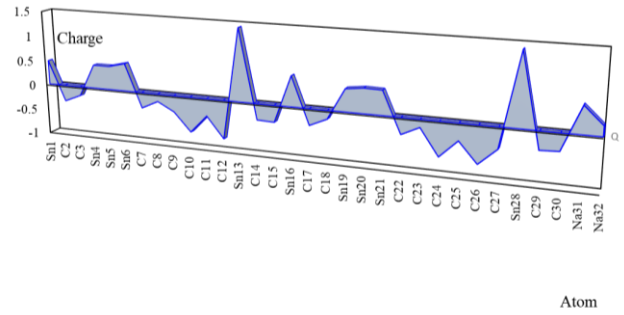

(b)

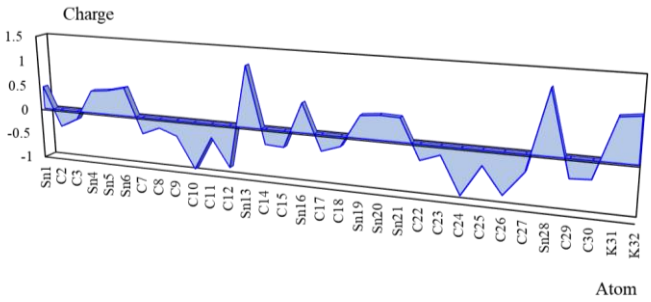

(c)

Figure 3. The changes of charge distribution (Coulomb) for **(a)** $SnLi^{+}C$; **(b)** $SnNa^{+}C$; **(c)** $SnK^{+}C$ nanoclusters.

3.2. Total density of states.

In an isolated system (such as a molecule), the energy levels are discrete; the concept of "density of state (DOS)" is supposed to be completely valueless in this situation. Therefore, the "original total DOS (TDOS)" of an isolated system can be written as [24] by the "Multiwfn" [25,26] program.

Regarding ion transport by $SnLi^{+}C$, $SnNa^{+}C$, and $SnK^{+}C$ nanoclusters, TDOS has been estimated (Figure 4a, b, c).

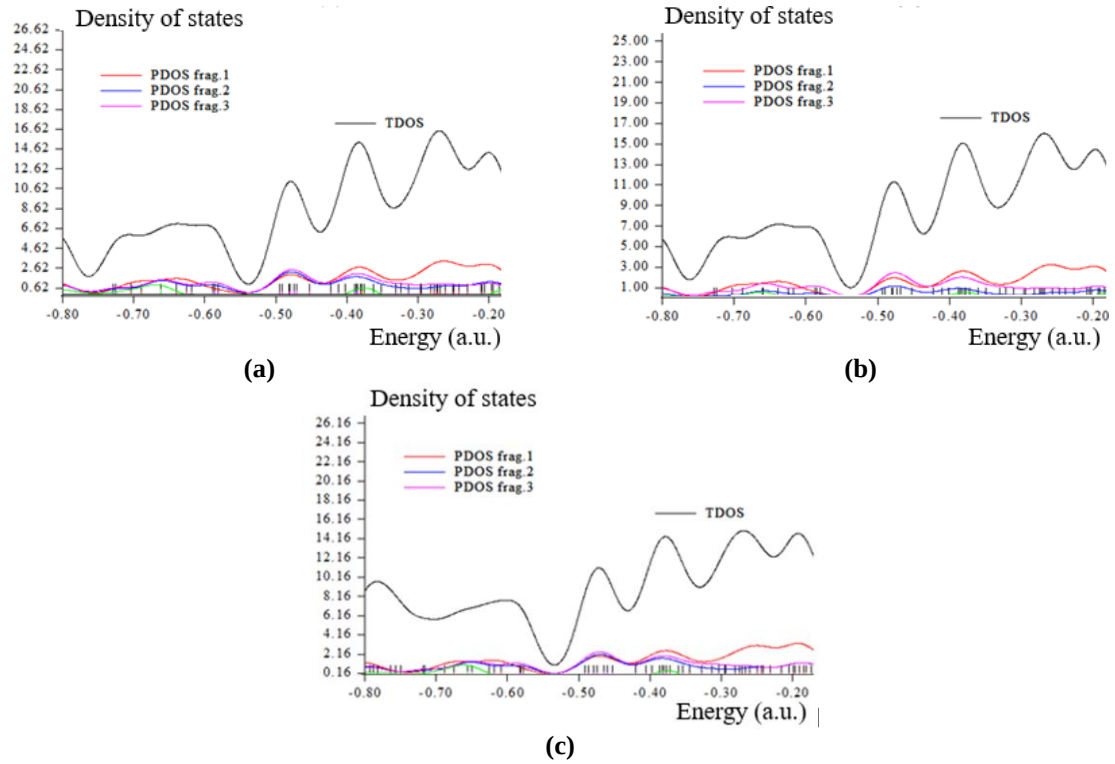

(a) **(b)**

(c)

Figure 4. PDOS/TDOS graphs of **(a)** $SnLi^{+}C$; **(b)** $SnNa^{+}C$; **(c)** $SnK^{+}C$ nanoclusters.

$SnLi^+C$, $SnNa^+C$, SnK^+C nanoclusters (Figure 4a,b,c) have shown the steepest maximum TDOS surrounding –0.30, –0.40, –0.50, and –0.60 a.u. owing to the covalent bond between Li^+, Na^+, K^+ cations and SnC nanostructure with a maximum density of state of ≈ 12.

Fragment 1 has been defined for C9 to C12, Si13, C24 to C27, Si28 and X31/X32 ($X=Li^+$, Na^+, K^+) in Figure 4 (a,b,c). Fragment 2 has indicated the fluctuation of Si1, Si4 to Si6 beside the similar involved atoms of Fragment 1 in Figure 4 (a,b,c). Finally, it was considered the fluctuation of Si16, Si19 to Si21, C17, C18, C22, C23, C29, C30 in Figure 4 (a,b,c).

3.3. Molecular electrostatic potential (ESP).

Trapping of Li^+, Na^+, and K^+ cations by SnC nanostructure (Figure 5a,b,c) towards formation of $SnLi^+C$, $SnNa^+C$, and SnK^+C nanoclusters might be described by molecular electrostatic potential (ESP) [27,28] graphs using Multiwfn [25,26] (Figure 5a,b,c).

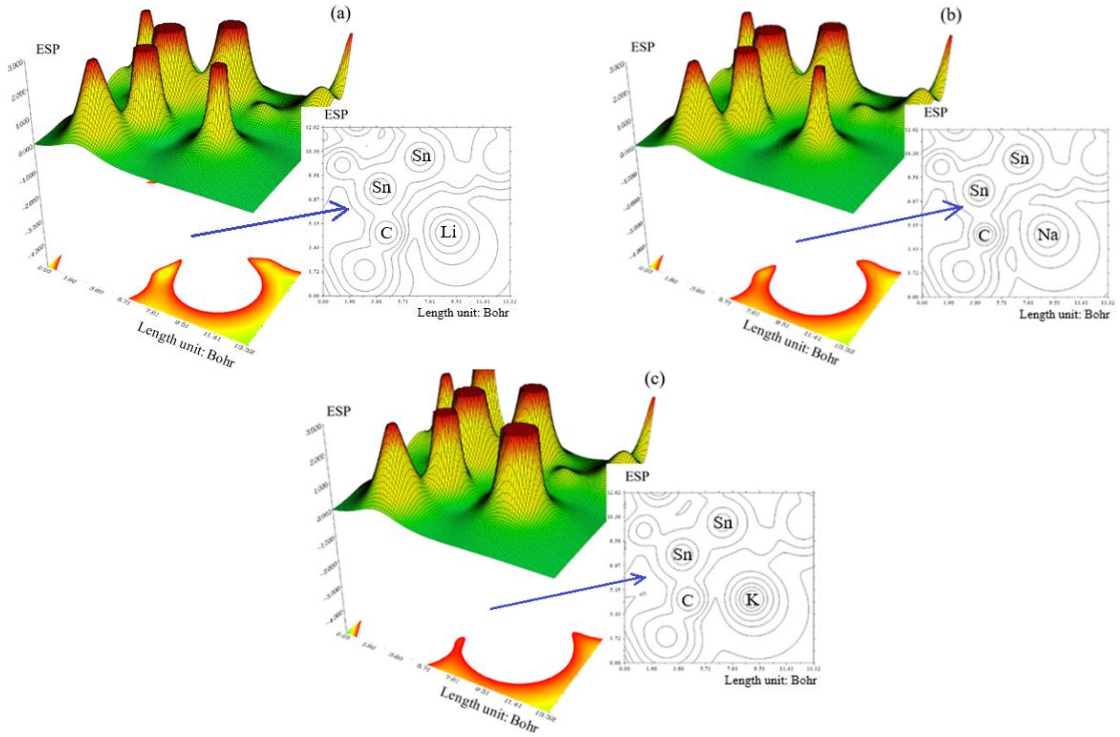

Figure 5. The counter (right side) and shaded (left side) maps of ESP graphs for **(a)** $SnLi^+C$; **(b)** $SnNa^+C$; **(c)** SnK^+C nanoclusters.

$SnLi^+C$ (Figure 5a), $SnNa^+C$ (Figure 5b), SnK^+C (Figure 5c) have illustrated the electron delocalization through an isosurface map with labeling atoms of C10, C12, Si13, C24, C26, Si28, X31/X32 ($X=Li^+$, Na^+, K^+). In fact, the counter map of ESP can confirm that $SnLi^+C$, $SnNa^+C$, and SnK^+C nanoclusters may augment the efficiency of ion transport (Figure 5a,b,c).

Table 2. Stability energy (kcal/mol), LUMO (eV), HOMO (eV), and energy gap (ΔE) (eV) for $SnLi^+C$, $SnNa^+C$, and SnK^+C nanoclusters.

Heteroclusters	$E_s \times 10^{-3}$ (kcal/mol)	E_{HOMO} (eV)	E_{LUMO} (eV)	$\Delta E = E_{LUMO} - E_{HOMO}$ (eV)
$SnLi^+C$	-503.7086	-4.9308	-3.8369	1.0938
$SnNa^+C$	-494.4563	-4.8556	-3.8121	1.0434
SnK^+C	-529.2968	-4.5833	-3.8474	0.7359

The layered tin carbide improved by alkali metal ions of lithium (1+), sodium (1+), and potassium (1+) has indicated the structural stability of Li^+-, Na^+-, and K^+-ion heteroclusters

through the reported stability energies in Table 2. The wavefunction level we used was CAM–B3LYP–D3/6–311+G(d,p) that corresponds to HOMO and LUMO, respectively (Table 2).

Therefore, E_{LUMO} (a.u.), E_{LUMO} (a.u.), and the local bandgap energies (ΔE/a.u.) and immobile charges induced by polarization discontinuity are simultaneously controlled throughout the structures, and optimized band profiles are eventually achieved for $SnLi^+C$, $SnNa^+C$, and SnK^+C nanoclusters (Table 2). As can be seen in Table 2, $SnLi^+C$ exhibits the largest energy gap (1.09 eV), implying higher stability; SnK^+C shows the lowest gap (0.73 eV), suggesting greater conductivity.

4. Conclusions

Functionalizing of Li^+, Na^+, K^+ cations can augment the negative atomic charge of C2, C3, C7–C12, C14, C15, C17, C18, C22–C27, C29, C30 as electron acceptors in $SnLi^+C$, $SnNa^+C$ and SnK^+C nanoclusters. $SnLi^+C$, $SnNa^+C$, SnK^+C nanoclusters have shown the steepest maximums TDOS surrounding –0.30, –0.40, –0.50, and –0.60 a.u. owing to the covalent bond between Li^+, Na^+, K^+ cations and SnC nanostructure with a maximum density of state of ≈ 12. The layered tin carbide improved by alkali metal ions of lithium (1+), sodium (1+), and potassium (1+) has indicated the structural stability of Li^+-, Na^+-, and K^+-ion heteroclusters through the reported stability energies. We presented that the ionic groups on the side chain of the nanocluster with smaller steric space should provide higher ionic conductivity due to their lower rotation energy barriers. This research article covers the state-of-the-art synthetic strategies for preparing the materials, the basic structure, and a panorama of different optimization strategies that lead to improved physicochemical properties.

Author Contributions

Conceptualization, F.M.; methodology, F.M.; software, F.M.; validation, F.M. and M.M.; formal analysis, F.M. and M.M.; investigation, F.M. and M.M.; resources, F.M. and M.M.; data curation, F.M.; writing—original draft preparation, F.M.; writing—review and editing, M.M.; visualization, F.M. and M.M.; supervision, F.M.; project administration. The author has read and agreed to the published version of the manuscript.

Institutional Review Board Statement

Not applicable.

Informed Consent Statement

Not applicable.

Data Availability Statement

Not applicable.

Funding

This research received no external funding.

Acknowledgments

In successfully completing this paper and its research, the authors are grateful to Kastamonu University.

Conflict of Interest

The author declares no conflict of interest.

References

1. He, L.; Long, X.; Zhang, C.; Ma, K.; She, L.; Mi, C.; Yu, M.; Xie, Z.; Wang, L. Direct Z-scheme β-SnSe/HfS_2 heterostructure for photocatalytic water splitting: High solar-to-hydrogen efficiency and excellent carrier mobility. *Mater. Today Commun.* **2024**, *38*, 108127, https://doi.org/10.1016/j.mtcomm.2024.108127.
2. Faye, O.; Szpunar, J.A. Effect of Metal Carbides on Hydrogen Embrittlement: A Density Functional Theory Study. *Hydrogen* **2024**, *5*, 137–148, https://doi.org/10.3390/hydrogen5010009.
3. Yang, D.; Zhang, X.; Nie, Y.; Zhu, H.; Xiang, G. Achieving highly efficient 2D SnC monolayer-based photocatalyst for water splitting via a synergistic strategy of S-scheme heterostructure construction and silicon doping. *Nanoscale* **2024**, *16*, 4866–4871, https://doi.org/10.1039/D3NR05453E
4. Zhou, S.; Mao, Y. First-Principles Study on Direct Z-Scheme SnC/SnS_2 Heterostructures for Photocatalytic Water Splitting. *Chemistry* **2025**, *7*, 76, https://doi.org/10.3390/chemistry7030076.
5. Luo, Y.-F.; Zhang, Y.; Li, J.-H.; Yang, Y.-S.; Sun, S.-Z.; Duan, L. The SnC/WS2 vdW heterojunction: A prospective direct Z-scheme photocatalyst for overall water decomposition with high STH efficiency and catalytic activity. *Mol. Catal.* **2024**, *557*, 113983, https://doi.org/10.1016/j.mcat.2024.113983.
6. Huang, Y.; Song, S.; Lian, J.; Cao, J.; Zheng, Y.; Wang, J.; Zhu, M.; Pan, J.; Li, C. Hollow cubic SnS2/CdS nanoheterojunction for enhanced photocatalytic hydrogen evolution and degradation via MOFs in situ sulfuration. *Int. J. Hydrogen Energy* **2024**, *64*, 1030–1039, https://doi.org/10.1016/j.ijhydene.2024.03.357
7. Cong, X.; Shah, M.N.U.; He, W. Straddling $SnSe_2$/SnS_2 van der Waals tunneling heterostructures for high performance broadband photodetectors. *J. Mater. Chem. C* **2024**, *12*, 5411–5419, https://doi.org/10.1039/D4TC00443D.
8. Mollaamin, F.; Monajjemi, M. Nanomaterials for Sustainable Energy in Hydrogen-Fuel Cell: Functionalization and Characterization of Carbon Nano-Semiconductors with Silicon, Germanium, Tin or Lead through Density Functional Theory Study. *Russ. J. Phys. Chem. B* **2024**, *18*, 607–623, https://doi.org/10.1134/S1990793124020271.
9. Liang, K.; Wang, J.; Wei, X.; Zhang, Y.; Yang, Y.; Liu, J.; Tian, Y.; Duan, L. Theoretical design of direct Z-scheme SnC/PtSe2 heterostructure with enhanced photocatalytic performance and tunable optoelectronic properties. *Phys. E* **2024**, *155*, 115825, https://doi.org/10.1016/j.physe.2023.115825.
10. Mollaamin, F. Anchoring of 2D layered materials of $Ge_5Si_5O_{20}$ for (Li/Na/K)-(Rb/Cs) batteries towards Eco-friendly energy storage. *BMC Chemistry* **2025**, *19*, 233, https://doi.org/10.1186/s13065-025-01593-0.
11. Rahman, S.; Sharme, R.K.; Terrones, M.; Rana, M.M. Recent Progress on Layered Sn and Pb-Based Mono Chalcogenides: Synthesis, Structure, Optical, and Thermoelectric Properties and Related Applications. *Nanomaterials* **2024**, *14*, 1530, https://doi.org/10.3390/nano14181530.
12. Yu, M.; Hilse, M.; Zhang, Q.; Liu, Y.; Wang, Z.; Law, S. Review of Nanolayered Post-transition Metal Monochalcogenides: Synthesis, Properties, and Applications. *ACS Appl. Nano Mater.* **2024**, *7*, 24, 28008–28026, https://doi.org/10.1021/acsanm.3c05984.
13. Lin, X.; Wan, R.; Zhang, Z.; Li, M.; Tian, G. Theoretical study of In2Sn2Se6 monolayer: A potential high-performance photocatalyst. *Surfaces and Interfaces* **2025**, *72*, 107300, https://doi.org/10.1016/j.surfin.2025.107300.
14. Zhou, S.; Mao, Y. First-Principles Study on Direct Z-Scheme SnC/SnS_2 Heterostructures for Photocatalytic Water Splitting. *Chemistry* **2025**, *7*, 76, https://doi.org/10.3390/chemistry7030076.
15. González-Barrios, M.; Tabuyo-Martínez, M.; Ávila-Brande, D.; Prado-Gonjal, J. Perspective on Crystal Structures, Synthetic Methods, and New Directions in Thermoelectric Materials. *Small Struct.* **2024**, 2400136, https://doi.org/10.1002/sstr.202400136.

16. Zhang, Z.; Liu, L.; Glenna, D.M.; Jana, A.; Pereza, C.M.; Qian, J. Real-space Kohn–Sham density functional theory for complex energy applications. *Chem. Commun*. **2025**, *61*, 10273–10286, https://doi.org/10.1039/D5CC01820J.
17. Mollaamin, F. Alkali Metals Doped on Tin-Silicon and Germanium-Silicon Oxides for Energy Storage in Hybrid Biofuel Cells: A First-Principles Study. *Russ. J. Phys. Chem. B* **2025**, *19*, 722–736, https://doi.org/10.1134/S1990793125700393.
18. Mu, L.; Jiang, J.; Gao, S.; Li, X.-Y.; Sheng, S. A DFT Study of Band-Gap Tuning in 2D Black Phosphorus via Li^+, Na^+, Mg^{2+}, and Ca^{2+} Ions. *Int. J. Mol. Sci.* **2024**, *25*, 11841, https://doi.org/10.3390/ijms252111841.
19. Czernek, J.; Brus, J. Reliable Dimerization Energies for Modeling of Supramolecular Junctions. *Int. J. Mol. Sci.* **2024**, *25*, 602, https://doi.org/10.3390/ijms25010602.
20. Zhou, X.; Cheng, Y.; Xu, X.; Zhang, L.; Tian, S.; Xu, X.; Guo, B.; Tang, W.; Yan, C.; Qian, T. Bader Charge Balance Mechanism Realizes Industrial-Grade Current Hydrogen Production. *Inorg. Chem.* **2025**, *64*, 14118–14127, https://doi.org/10.1021/acs.inorgchem.5c00590.
21. Frisch, M.J.; Trucks, G.W.; Schlegel, H.B.; Scuseria, G.E.; Robb, M.A.; Cheeseman, J.R.; Scalmani, G.; Barone, V.; Petersson, G.A.; Nakatsuji, H.; Li, X.; Caricato, M.; Marenich, A.V.; Bloino, J.; Janesko, B.G.; Gomperts, R.; Mennucci, B.; Hratchian, H.P.; Ortiz, J. V.; Izmaylov, A. F.; Sonnenberg, J.L.; Williams-Young, D.; Ding, F.; Lipparini, F.; Egidi, F.; Goings, J.; Peng, B.; Petrone, A.; Henderson, T.; Ranasinghe, D.; Zakrzewski, V.G.; Gao, J.; Rega, N.; Zheng, G.; Liang, W.; Hada, M.; Ehara, M.; Toyota, K.; Fukuda, R.; Hasegawa, J.; Ishida, M.; Nakajima, T.; Honda, Y.; Kitao, O.; Nakai, H.; Vreven, T.; Throssell, K.; Montgomery, J.A., Jr.; Peralta, J.E.; Ogliaro, F.; Bearpark, M.J.; Heyd, J.J.; Brothers, E.N.; Kudin, K.N.; Staroverov, V.N.; Keith, T.A.; Kobayashi, R.; Normand, J.; Raghavachari, K.; Rendell, A.P.; Burant, J.C.; Iyengar, S.S.; Tomasi, J.; Cossi, M.; Millam, J.M.; Klene, M.; Adamo, C.; Cammi, R.; Ochterski, J.W.; Martin, R.L.; Morokuma, K.; Farkas, O.; Foresman, J.B.; Fox, D.J. Gaussian 16, Revision C.01, Gaussian, Inc., Wallingford CT, **2016**.
22. Dennington, R.; Keith Todd, A.; Millam John, M. GaussView, Version 6.06.16. Semichem Inc., Shawnee Mission, KS, USA, **2016**.
23. Xu, Z.; Qin, C.; Yu, Y.; Jiang, G.; Zhao, L. First-principles study of adsorption, dissociation, and diffusion of hydrogen on α-U (110) surface. *AIP Adv.* **2024**, *14*, 055114, https://doi.org/10.1063/5.0208082.
24. Rukelj, Z.; Kupčić, I.; Radić, D. Density of States in the 3D System with Semimetallic Nodal-Loop and Insulating Gapped Phase. *Symmetry* **2024**, *16*, 38, https://doi.org/10.3390/sym16010038.
25. Lu, T.; Chen, F. Multiwfn: A multifunctional wavefunction analyzer. *J. Comput. Chem.* **2012**, *33*, 580–592, https://doi.org/10.1002/jcc.22885.
26. Lu, T. A comprehensive electron wavefunction analysis toolbox for chemists, Multiwfn. *J. Chem. Phys.* **2024**, *161*, 082503, https://doi.org/10.1063/5.0216272.
27. Murray, J.S.; Riley, K.E.; Brinck, T. A Revival of Molecular Surface Electrostatic Potential Statistical Quantities: Ionic Solids and Liquids. *Crystals* **2024**, *14*, 995, https://doi.org/10.3390/cryst14110995.
28. Matta, C.F.; Ayers, P.W.; Cook, R. The Physics of Electron Localization and Delocalization. In Electron Localization-Delocalization Matrices, Matta, C.F., Ayers, P.W., Cook, R., Eds.; Springer International Publishing: Cham, **2024**; 7–20, https://doi.org/10.1007/978-3-031-51434-0_2.

Publisher's Note & Disclaimer